IEEE Access
Multidisciplinary ⋮ Rapid Review ⋮ Open Access Journal

Received January 4, 2022, accepted January 19, 2022, date of publication January 28, 2022, date of current version February 7, 2022.

Digital Object Identifier 10.1109/ACCESS.2022.3147507

Neutral Voltage Modulation for Maximizing the Linear Modulation Region and Limp-Home Mode Operation of Multilevel Cascaded Inverters Under DC-Link Imbalance Conditions

JEONGWOO KIM, (Member, IEEE), AND YOUNGHOON CHO, (Member, IEEE)
Department of Electrical and Electronics Engineering, Konkuk University, Seoul 05029, South Korea
Corresponding author: Younghoon Cho (yhcho98@konkuk.ac.kr)

This work was supported by Konkuk University, in 2018.

ABSTRACT This paper proposes an improved neutral voltage modulation (NVM) method for symmetrical and asymmetrical three-phase multilevel cascaded inverters (MLCIs). The maximum synthesizable space vector region is analyzed using the number of healthy inverter modules and the amplitudes of the dc-link voltages in each phase. After that, the NVM strategy is proposed to maximize the balanced three-phase output voltages in the given space vector region. The proposed method matches the polarities of the neutral and the phase voltage references as well as minimizing the neutral voltage. By using the proposed method, the linear modulation region of the three-phase MLCI are fully utilized allowing no overmodulations even under severe dc-link voltage imbalances. Moreover, the proposed NVM can synthesizes rotating voltage vectors even all modules of one phase are not available. To verify the effectiveness of the proposed method, a two-by-three MLCI prototype is built and tested. The experimental results show that the proposed method reduces the total harmonic distortion (THD) and the ripple component of the phase current by 28% and 32.8%, respectively, compared to traditional modulation strategies under severe dc-link imbalance conditions.

INDEX TERMS Fault tolerance, multilevel cascaded inverters, neutral voltage modulation, space vector pulse width modulation.

I. INTRODUCTION

Multilevel inverters (MLIs) have many advantages over two-level inverters. MLIs' various structures and modulation techniques allow them to have more output voltage levels than two-level inverters, so their output waveform has lower harmonic distortion [1]. In addition, the voltage stress across the switching devices in MLIs are lower than two-level inverters at the same dc-link level [2], [3]. MLIs are also attractive for high voltage applications, because they can be constructed by stacking low voltage modules [2], [4]–[6]{Deepa, 2018 #8;J. Rodriguez, Nov. 2009 #6;M. Vijeh, Oct. 2019 #1}. From the reasons above, MLIs are utilized in various industrial applications such as static synchronous compensators, battery energy storage systems, power plants, and so on [7]–[10]. The topologies of MLIs can be roughly categorized as neutral point clamped and cascaded types [11], [12]. In MLIs' topologies, multilevel cascaded inverters (MLCIs) are suitable for modular structures. This modular approach allows MLCIs can easily increase output power and voltage levels by adding more inverter modules. In addition, the modular MLCI can easily implement a fault tolerant operation when a single or multiple modules are under faulty conditions [13], [14]. This is a significant advantage of the modular MLCI structure, and a lot of research has been conducted on this issue.

One simple approach to implement fault tolerant operation is bypassing the abnormal module as shown in Fig. 1. However, the line-to-line voltage may be unbalanced if there is no dedicated modulation strategy at that condition. Moreover, the voltage utilization of healthy modules may be significantly harmed. To resolve these issues, a lot of research including circuits and algorithm approaches have been conducted. Several methods using redundant modules were proposed to improve the performance of MLCI under faulty conditions [15], [16]. Some redundant modules can

The associate editor coordinating the review of this manuscript and approving it for publication was Pinjia Zhang.

be alternatively replaced with faulty modules for the post-fault operation. These methods maintain the output voltage level as normal conditions, but the total system design may be inefficient due to the existence of extra redundant modules.

To overcome this drawback, other fault-tolerant operation methods without extra modules have been proposed. In [17]–[19], neutral-shift strategies were introduced. In the neutral-shift methods, the magnitude and phase of three-phase references are modified to move the neutral point of three-phase MLCI when faulty modules are bypassed. As a result, three-phase output power becomes balanced. However, the voltage utilization may not be maximized in specific fault conditions in these methods. To compensate this disadvantage, the improved neutral-shift methods were proposed in [20]–[22]. In addition, there are attempts to combine the neutral point shift method with selective harmonic elimination based pulse width modulation [23]. However, these methods require either lookup tables or complex calculations for solving nonlinear equations.

Such burdens can be mitigated by fault-tolerant strategies based on zero-sequence injection strategies [24]–[29]. In these methods, the neutral point of the power converter is moved in faulty module conditions by injecting the zero-sequence voltage which contains the fundamental frequency. As a result, it enables the MLCI to maintain continuous operation as well as synthesizing a balanced three-phase line-to-line voltage [24]–[26]. However, the three-phase MLCI may undergo the overmodulation when the operating condition is near the maximum duty references [27]. To reduce the effect of the overmodulation, the closed-loop zero-sequence voltage injection method are proposed in [28], [29]. These methods allow the three-phase MLCI to achieve the balanced line-to-line voltage without overmodulation in steady-state. However, it requires additional effort such as a closed-loop error minimization algorithm allowing no harmonic components in the zero-sequence voltage.

On the other hand, another neutral point shift method using neutral voltage modulation (NVM) is proposed in [30]–[32]. In NVM methods, the neutral voltage reference for the voltage between the inverter and load side neutral points is calculated based on the number of the healthy modules and the phase voltage references [30]. Then, the neutral voltage reference is added to each three-phase reference to move the neutral point. In [31], the neutral voltage reference is calculated to reduce the total harmonic distortion (THD) of the current and its harmful effect on motor components. Reference [32] proposes the NVM strategy for asymmetrical MLCI under unbalanced dc-link voltage conditions. In the paper, the neutral voltage reference is directly calculated from the phase voltage references and available dc-link voltages. However, the NVM method proposed in [32] may occur overmodulation when the pole voltage reference calculated by subtracting the neutral voltage reference from phase voltage reference exceeds the magnitude of the dc-link voltage. In addition, this NVM method cannot be directly applied if all modules of one phase are not available, because the NVM method should utilize the number of remaining modules while calculating the neutral voltage reference.

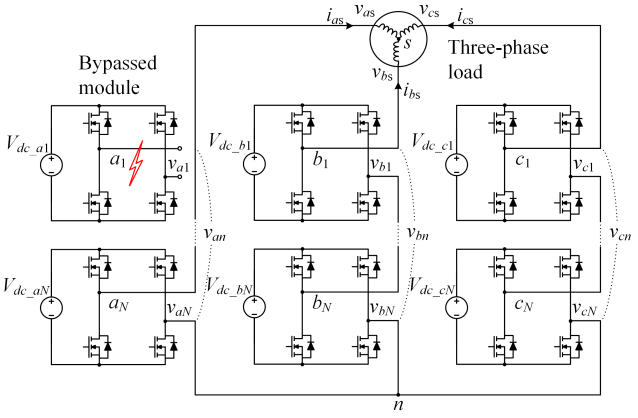

FIGURE 1. Three-phase MLCI topology with three-phase load when one faulty module in a phase leg is bypassed.

In this paper, an NVM method is proposed to obtain a balanced three-phase output of MLCI in the maximum modulation region with minimizing overmodulation. Initially, to recognize the maximum synthesizable voltage of the three-phase MLCI under normal and abnormal conditions, space voltage vectors are analyzed in the stationary $\alpha\beta$ reference frame. Then, the neutral voltage reference is calculated by using the proposed method to avoid the overmodulation in the pole voltage references. Moreover, the proposed NVM can be applied when all modules in one phase are unavailable. Experimental results are presented to verify the performance of the proposed method for two-by-three MLCI under unbalanced module conditions.

II. SPACE VOLTAGE VECTOR ANALYSIS

A. SYMMETRICAL CONDITIONS

Fig. 1 shows the N-by-three MLCI structure. In the figure, the individual dc-links of each module are defined as V_{dc_pk} where p and k designate the name of the individual phase and the number of the modules in the dedicated phase. For example, V_{dc_a2} stands for the dc-link voltage of the second module in phase a. By considering this notation, the total dc-link voltage of a phase is:

$$V_{dc\_p} = \sum_{k=1}^{N} V_{dc\_pk|p\in(a,b,c)} \tag{1}$$

where N is the number of modules in the phase.

Let us define the phase voltages v_{as}, v_{bs}, and v_{cs} as the voltages between the switching pole in each phase and the load side neutral point s as shown in Fig. 1. Similarly, the pole voltages v_{an}, v_{bn}, and v_{cn} are defined as the output voltages between the switching poles and the inverter side neutral point n. The relationships between the phase and the pole voltages are written in (2).

$$\begin{aligned} v_{an} &= v_{as} + v_{sn} \\ v_{bn} &= v_{bs} + v_{sn} \\ v_{cn} &= v_{cs} + v_{sn} \end{aligned} \tag{2}$$

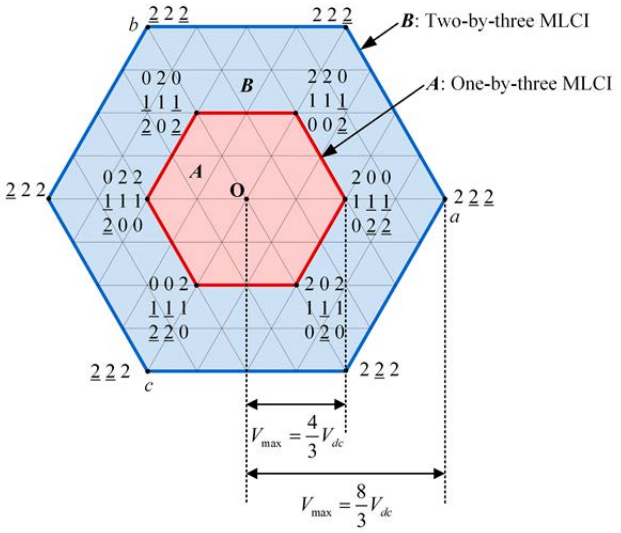

FIGURE 2. Comparison of space voltage vectors in one-by-three and two-by-three MLCIs.

where v_{sn} is defined as the neutral voltage between the neutral points s and n. By introducing the existence function S_{pk} for the single H-bridge module, the elements of S_{pk} are:

$$S_{pk} \in \{-1,\ 0,\ 1\} \tag{3}$$

where p and k are the same notation which is defined above. Using S_{pk} and V_{dc_pk}, the pole voltage of a phase is written as:

$$v_{pn} = \sum_{k=1}^{N} S_{pk} V_{dc\_pk}. \tag{4}$$

Since (2) meets Kirchhoff's voltage law, v_{sn} is obtained as:

$$v_{sn} = \frac{1}{3}(v_{an} + v_{bn} + v_{cn}). \tag{5}$$

By manipulating the equations above, the individual phase voltages are represented as follows.

$$\begin{bmatrix} v_{as} \\ v_{bs} \\ v_{cs} \end{bmatrix} = \frac{1}{3}\begin{bmatrix} 2 & -1 & -1 \\ -1 & 2 & -1 \\ -1 & -1 & 2 \end{bmatrix}\begin{bmatrix} v_{an} \\ v_{bn} \\ v_{cn} \end{bmatrix} \tag{6}$$

Using Clarke's transform, (6) can be written as:

$$\begin{bmatrix} v_{\alpha} \\ v_{\beta} \end{bmatrix} = \frac{1}{3}\begin{bmatrix} 2 & -1 & -1 \\ 0 & \sqrt{3} & -\sqrt{3} \end{bmatrix}\begin{bmatrix} v_{an} \\ v_{bn} \\ v_{cn} \end{bmatrix}. \tag{7}$$

Through (4) to (7), when the dc-link voltages of each module are the same as V_{dc}, the maximum synthesizable phase voltage of the symmetrical three-phase MLCI is obtained as:

$$V_{max} = \frac{4N}{3} \times V_{dc} \tag{8}$$

Meanwhile, the maximum achievable phase voltage in the linear modulation region is calculated as follows.

$$V_{ph\_max} = \frac{2N}{\sqrt{3}} V_{dc} \tag{9}$$

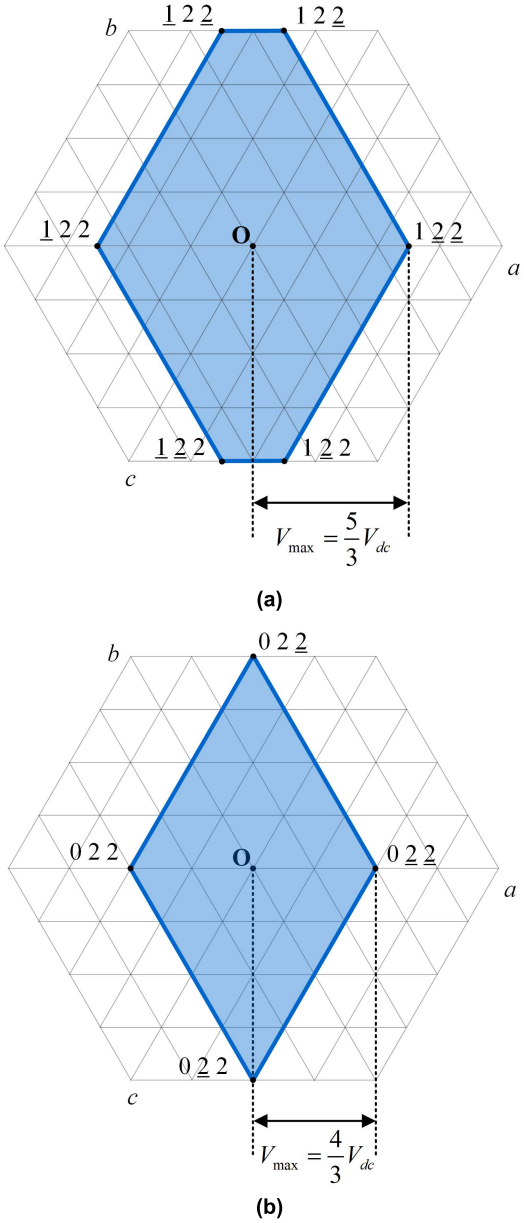

FIGURE 3. Space vector regions in asymmetrical conditions. (a) $V_{dc\_a} = 0.5V_{dc}$, $V_{dc\_b} = 2V_{dc}$, and $V_{dc\_c} = 2V_{dc}$. (b) $V_{dc\_a} = 0$, $V_{dc\_b} = 2V_{dc}$, and $V_{dc\_c} = 2V_{dc}$.

Fig. 2 compares the space voltage vectors for the symmetrical one-by-three and two-by-three MLCIs. In the figure and hereafter, underlined numbers indicate the negative switching elements -1 or -2. For two-by-three MLCIs where N is 2, $V_{\max}$ is calculated as $8V_{dc}/3$ using (8). On the other hand, $V_{\max}$ is reduced to $4V_{dc}/3$ in one-by-three MLCI. Accordingly, the linear modulation region also proportionally shrinks.

B. ASYMMETRICAL CONDITIONS

In asymmetrical three-phase MLCI, total dc-link voltages of each phase are unequal, because the number of normal modules and dc-link voltage of each module are different. Let us define the faulty module index f_{pk} for individual

phase and modules as follows:

$$f_{pk} = \begin{cases} 1, & \text{normal condition} \\ 0, & \text{bypassed condition.} \end{cases} \quad (10)$$

For example, if f_{a2} is 0, the module 2 in phase a is bypassed. By utilizing the faulty module index, the total dc-link voltages of each phase V_{dc_a}, V_{dc_b}, and V_{dc_c} in the two-by-three MLCI can be represented as:

$$\begin{aligned} V_{dc\_a} &= f_{a1}V_{dc\_a1} + f_{a2}V_{dc\_a2} \\ V_{dc\_b} &= f_{b1}V_{dc\_b1} + f_{b2}V_{dc\_b2} \\ V_{dc\_c} &= f_{c1}V_{dc\_c1} + f_{c2}V_{dc\_c2} \end{aligned} \quad (11)$$

By using the independent and the dependent vectors concepts [32], $V_{\max}$ and $V_{\text{ph\_max}}$ in asymmetrical MLCIs are derived as:

$$V_{max} = \frac{2}{3}\left(V_{dc\_mid} + V_{dc\_min}\right) \quad (12)$$

$$V_{ph\_max} = \frac{V_{dc\_mid} + V_{dc\_min}}{\sqrt{3}} \quad (13)$$

where V_{dc_mid} and V_{dc_min} represent the medium and minimum values among V_{dc_a}, V_{dc_b}, and V_{dc_c} which are determined by (11). Fig. 3 illustrates the space vector regions of the asymmetrical two-by-three MLCI for different dc-link voltage cases. In Fig. 3(a), V_{dc_mid} and V_{dc_min} are $2V_{dc}$ and $0.5V_{dc}$, respectively. Hence, V_{max} and V_{ph_max} are calculated as $5V_{dc}/3$ and $2.5V_{dc}/\sqrt{3}$. Similarly, V_{max} and V_{ph_max} are obtained as $4V_{dc}/3$ and $2V_{dc}/\sqrt{3}$ for Fig. 3(b). It should be noticed that the MLCI can secure the space voltage vectors as shown in Fig. 3(b) when even whole dc-link in a phase is not available, so that rotating voltage vectors can be produced. Another aspect to be mentioned is that asymmetrical six or four-step operation can be implemented in the MLCI according to the dc-link conditions.

III. PROPOSED MODULATION STRATEGY

Fig. 4 represents the block diagram of the proposed method which consists of two steps for implementation. First, the phase voltage reference and the dc-link values are utilized to generate the neutral voltage v'_{sn} to balance out the three-phase references. After that, v'_{sn} is recalculated to maximize the linear modulation region. As the result of the second step, v''_{sn} is produced, and it is injected to the phase voltage references. Finally, the pole voltage references are calculated and commanded.

A. ANALYSIS OF THE TRADITIONAL TECHNIQUE

The neutral voltage reference followed by [32] can be calculated based on the phase voltage references and dc-link voltages in each phase. Initially, the weight factor K_w considering the dc-link voltages can be defined as:

$$K_w = \frac{V_{dc\_mid} + V_{dc\_min}}{2} \quad (14)$$

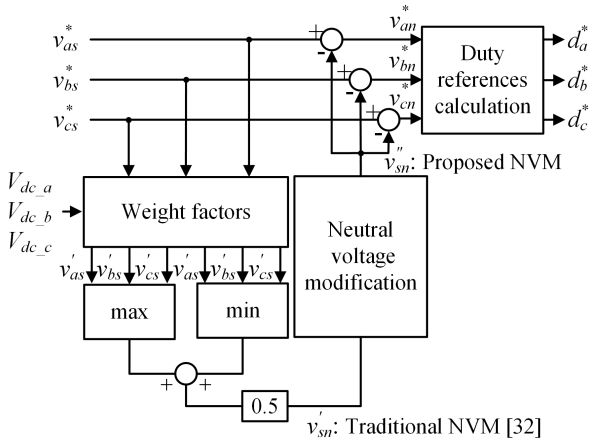

FIGURE 4. Proposed NVM technique with the neutral voltage modification.

The weight factors of each phase, K_{w_a}, K_{w_b}, and K_{w_c}, are written as follows:

$$K_{w\_a} = \frac{K_w}{V_{dc\_a}} \quad K_{w\_b} = \frac{K_w}{V_{dc\_b}} \quad K_{w\_c} = \frac{K_w}{V_{dc\_c}}. \quad (15)$$

After that, they are multiplied to the original phase voltage references v^*_{as}, v^*_{bs}, and v^*_{cs} as (16).

$$v'_{as} = K_{w\_a}v^*_{as} \quad v'_{bs} = K_{w\_b}v^*_{bs} \quad v'_{cs} = K_{w\_c}v^*_{cs}. \quad (16)$$

Here, the neutral voltage reference v'_{sn} is calculated as:

$$v'_{sn} = \frac{v'_{max} + v'_{min}}{2} \quad (17)$$

where v'_{max} and v'_{min} are the maximum and the minimum values among v'_{as}, v'_{bs}, and v'_{cs}. It should be noticed that v'_{sn} includes the weighted neutral voltage considering the dc-link imbalance in three-phase. Now, the pole voltage references are calculated as:

$$\begin{bmatrix} v^*_{an} \\ v^*_{bn} \\ v^*_{cn} \end{bmatrix} = \begin{bmatrix} v^*_{as} - v'_{sn} \\ v^*_{bs} - v'_{sn} \\ v^*_{cs} - v'_{sn} \end{bmatrix}. \quad (18)$$

Let us examine the physical meaning of the modulation method above with following analyses. For the first case, assume that $V_{dc\_a} = V_{dc}$, $V_{dc\_b} = 2V_{dc}$, and $V_{dc\_c} = 3V_{dc}$. Then, the weight factors of each phase are:

$$K_{w\_a} = 1.5 \quad K_{w\_b} = 0.75 \quad K_{w\_c} = 0.5. \quad (19)$$

From (19), it is confirmed that the weight factor of the minimum dc-link leg, phase a, is greater than 1 while the weight factors of other phases are less than 1. Thus, the relationships among the original and the modified phase voltage references become:

$$\left|v'_{as}\right| > \left|v^*_{as}\right| \quad \left|v'_{bs}\right| < \left|v^*_{bs}\right| \quad \left|v'_{cs}\right| < \left|v^*_{cs}\right|. \quad (20)$$

Hence, when v'_{as} corresponds to v'_{max} or v'_{min}, the peak value of v'_{sn} is increased by (16) and (17), so that the peak magnitude of v^*_{an} is less than its original phase voltage reference by (18). On the other hand, when v'_{cs} corresponds to v'_{max} or v'_{min}, the

peak value of v'_{sn} is reduced, and the peak of v^*_{cn} is higher than v^*_{cs}. In sum, the peak of the pole voltage reference with the minimum dc-link phase decreases whereas the one with the maximum dc-link phase increases. Hence, the balanced voltage output of MLCI is achieved as well as supplying fair output power.

For the next, assume that the dc-link voltages in each phase are equal to V_{dc}. Then, the weight factors and phase voltage references are:

$$\begin{aligned} K_w &= V_{dc} \\ K_{w\_a} &= K_{w\_b} = K_{w\_c} = 1 \\ v'_{as} &= v^*_{as}, \quad v'_{bs} = v^*_{bs}, \; v'_{cs} = v^*_{cs}. \end{aligned} \tag{21}$$

In this case, the shape of v'_{sn} is identical to the one of the well-known carrier-based space vector PWM (SVPWM) case.

One problem of this modulation method is the possibility that the pole voltage reference can exceed its dc-link voltage, and have an opposite polarity compared to its original voltage reference. To analyze in detail, let us consider that $V_{dc\_a} < V_{dc\_b} < V_{dc\_c}$. From the above examination, v'_{sn} increases when v'_{as} corresponds to v'_{max} or v'_{min}. In this condition, the peak magnitude of v^*_{an} decreases, while the peak magnitude of v^*_{bn} and v^*_{cn} increase. Hence, if v^*_{bn} and v^*_{cn} exceed V_{dc_b} and V_{dc_c}, the overmodulation is happened. Regarding the magnitudes of dc-link voltages, V_{dc_b} is relatively lower than V_{dc_c}, so that the possibility of overmodulation occurrence is high in phase b. Therefore, the boundary condition of overmodulation can be derived by calculating the peak magnitude of v^*_{bn} when the original phase voltage references are as follows:

$$\begin{aligned} v^*_{as} &= V_{ph\_max} \sin \omega t \\ v^*_{bs} &= V_{ph\_max} \sin (\omega t - 2\pi/3) \\ v^*_{cs} &= V_{ph\_max} \sin (\omega t + 2\pi/3) \end{aligned} \tag{22}$$

where ω is the angular frequency of the output voltage. When $v'_{max} = v'_{as}$, and $v'_{min} = v'_{bs}$, v^*_{bn} is calculated as:

$$v^*_{bn} = v^*_{bs} - v'_{sn} = k_1 \sin \omega t + k_2 \sin (\omega t - 2\pi/3) \tag{23}$$

where k_1 and k_2 are:

$$\begin{aligned} k_1 &= -\frac{\left(V_{dc\_mid} + V_{dc\_min}\right)^2}{4\sqrt{3}\, V_{dc\_min}} \\ k_2 &= \frac{\left(V_{dc\_mid} + V_{dc\_min}\right)}{\sqrt{3}} - \frac{\left(V_{dc\_mid} + V_{dc\_min}\right)^2}{4\sqrt{3}\, V_{dc\_mid}}. \end{aligned} \tag{24}$$

Thus, the peak magnitude of v^*_{bn} is derived as:

$$v^*_{bn\_max} = \sqrt{k_1^2 - k_1 k_2 + k_2^2}. \tag{25}$$

As a result, the overmodulation occurs when the value of (25) exceeds V_{dc_b}. On the other hand, in the same dc-link voltage condition, v^*_{an} decreases as v'_{sn} increases. Therefore, v^*_{an} can have different polarity with v^*_{as}. This condition is derived in [32] as $V_{dc\_min} > V_{dc\_mid}/3$.

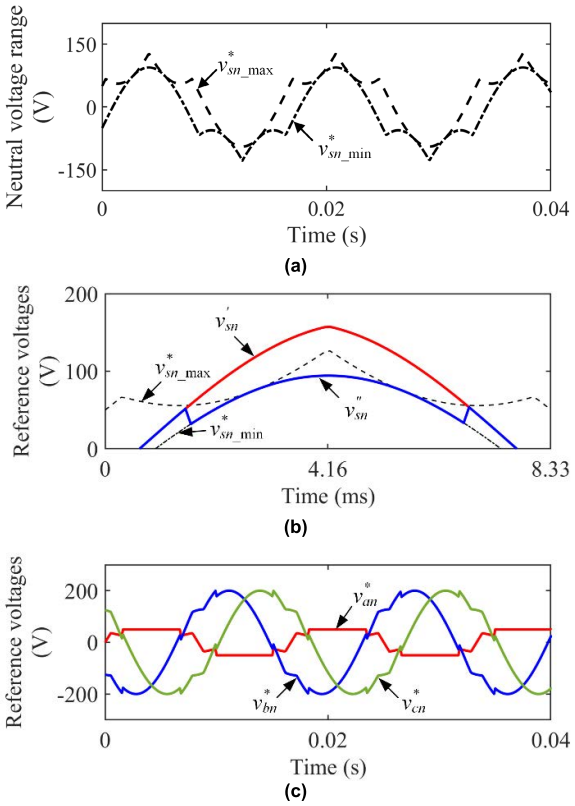

FIGURE 5. Waveforms of the modified NVM with $V_{dc_a} = 50$V, $V_{dc_b} = 200$V, and $V_{dc_c} = 200$V. (a) Injectable neutral voltage range (b) Comparison of the neutral voltage references. (c) Pole voltage references.

B. PROPOSED NVM TECHNIQUE

To avoid the operating in the overmodulation region, the modified NVM algorithm is proposed. In the proposed method, the neutral voltage reference v'_{sn} is modified considering the constraint regions. To prevent the overmodulation regions, the neutral voltage should be limited in the ranges as follows [22].

$$v^*_{sn\_min} < v'_{sn} < v^*_{sn\_max} \tag{26}$$

Here, the minimum and maximum values of the neutral voltage references, $v^*_{sn\_min}$ and $v^*_{sn\_max}$ are obtained as:

$$\begin{aligned} v^*_{sn\_min} &= \max(v^*_{as} - V_{dc\_a}, v^*_{bs} - V_{dc\_b}, v^*_{cs} - V_{dc\_c}) \\ v^*_{sn\_max} &= \min(v^*_{as} + V_{dc\_a}, v^*_{bs} + V_{dc\_b}, v^*_{cs} + V_{dc\_c}). \end{aligned} \tag{27}$$

Fig. 5(a) shows the range of the available neutral voltage reference when the magnitude of the phase voltage reference is V_{ph_max}, and the number of each phase are $V_{dc_a} = 50$V, $V_{dc_b} = 200$V, and $V_{dc_c} = 200$V. When the neutral voltage reference exceeds the ranges defined in (26), the proposed method selects the neutral voltage reference according to the conditions as follows:

$$v''_{sn} = \begin{cases} v^*_{sn\_min}, & \text{if } v'_{sn} > v^*_{sn\_max} \\ v^*_{sn\_max}, & \text{if } v'_{sn} < v^*_{sn\_min} \\ v'_{sn}, & \text{if } v^*_{sn\_min} < v'_{sn} < v^*_{sn\_max}. \end{cases} \tag{28}$$

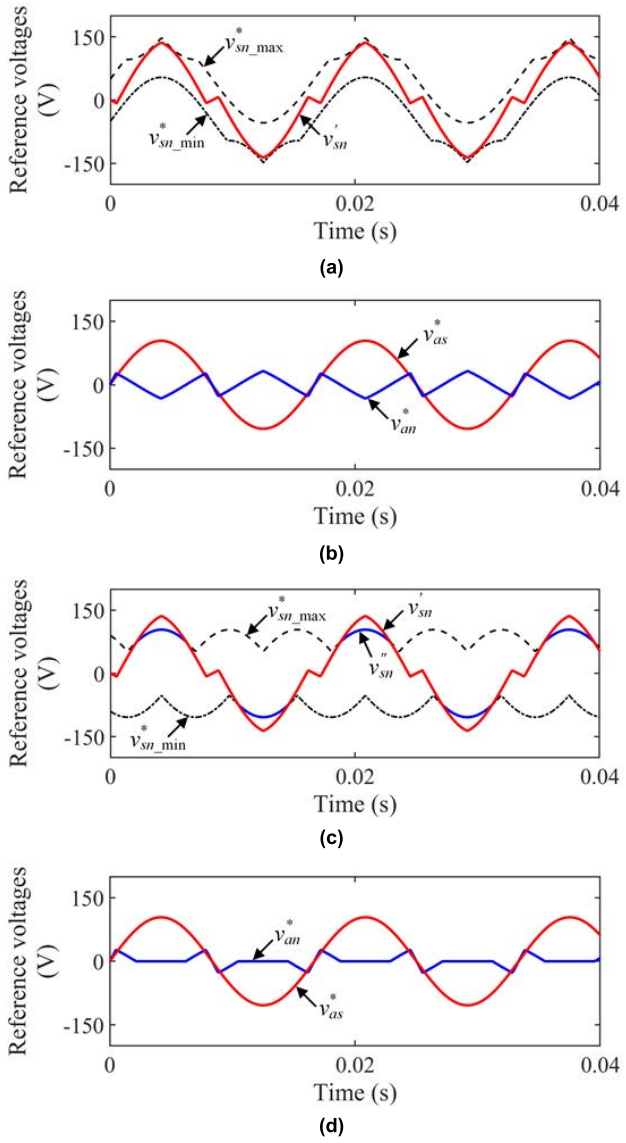

FIGURE 6. Waveforms of the modified NVM with $V_{dc\_a} = 50V$, $V_{dc\_b} = 200V$, and $V_{dc\_c} = 200V$. (a) Neutral Reference voltage without (29) (b) Reference voltages without (29) (c) Comparison of the neutral voltage references. (d) Reference voltages with (29).

Fig. 5(*b*) compares the original neutral voltage reference v'_{sn} generated by the algorithm suggested in [32] and the new neutral voltage reference v''_{sn} in the proposed method. Apparently, v'_{sn} is higher than $v^*_{sn\_max}$ in the figure while v''_{sn} does not violate the condition in (26). Let us consider the pole voltage references which include both the phase and neutral voltage references. The pole voltage references in Fig. 5(*c*) clearly indicate that no overmodulation is appeared due to the operation of the proposed algorithm.

From modified NVM method in (28), the overmodulation regions are disappeared. However, the pole voltage references can have the different polarity with the phase voltage references when (28) is applied. For example, Fig. 6(*a*) shows that v'_{sn} is still in the range of (26) when the amplitude of phase voltage reference is $0.6V_{ph\_max}$. In the same condition, v^*_{an} has

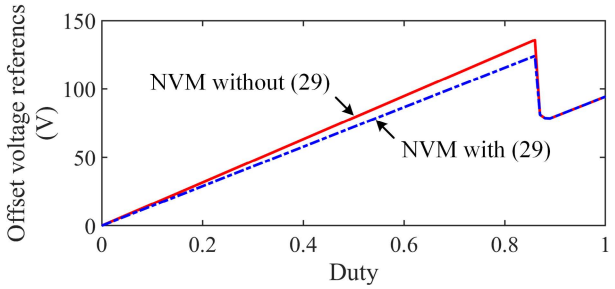

FIGURE 7. Comparison of the amplitude of neutral voltage references NVM with $V_{dc\_a} = 50V$, $V_{dc\_b} = 200V$, and $V_{dc\_c} = 200V$.

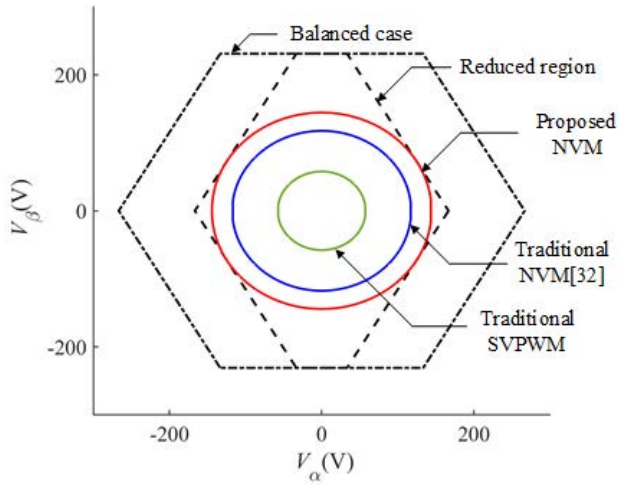

FIGURE 8. Comparison of the maximum linear modulation region with $V_{dc\_a} = 50V$, $V_{dc\_b} = 200V$, and $V_{dc\_c} = 200V$.

different polarity with v^*_{as} shown in Fig. 6(*b*). This is because v'_{sn} is larger than v^*_{as}, and the excessive v'_{sn} can be simply modified by (29).

$$v''_{sn} = \begin{cases} v^*_{max}, & \text{if } v'_{sn} > v^*_{max} \\ v^*_{min}, & \text{if } v'_{sn} < v^*_{min} \\ v'_{sn}, & \text{if } v^*_{min} < v'_{sn} < v^*_{max} \end{cases}$$
$$v^*_{max} = \max(v^*_{as}, v^*_{bs}, v^*_{cs}) \quad v^*_{min} = \min(v^*_{as}, v^*_{bs}, v^*_{cs}) \quad (29)$$

In Fig. 6(*c*), v'_{sn} is limited to the v^*_{min} or v^*_{max} when v'_{sn} exceeds the range of (29). As a result, v^*_{an} has the same polarity with v^*_{as} depicted in Fig. 6(*d*). In addition, the magnitude of the neutral voltage reference is reduced after (29) is applied as shown in Fig. 7. When the duty reference is 0.86, the maximum magnitude of the neutral voltage reference with (29) decreases from 135.8V to 124.1V. This can also reduce the harmful effect of the large neutral voltage on the motor components such as bearings [23].

Fig. 8 compares the maximum linear modulation regions of the traditional SVPWM, the traditional NVM suggested in [32], and the proposed NVM method. The maximum linear modulation region of the proposed NVM is adjacent to the maximum synthesizable voltage vector space region. On the other hand, the radius of the maximum linear modulation region is only 60% and 18.6% with the traditional NVM

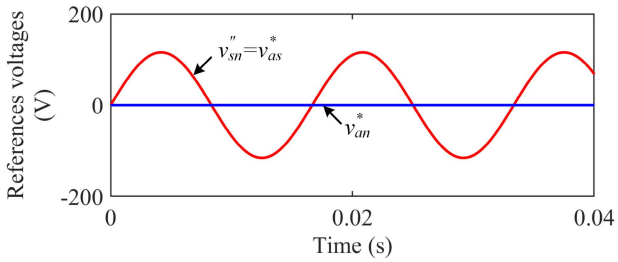

FIGURE 9. Waveform of the proposed NVM voltage references with $V_{dc_a} = 0$V, $V_{dc_b} = 200$V, and $V_{dc_c} = 200$V.

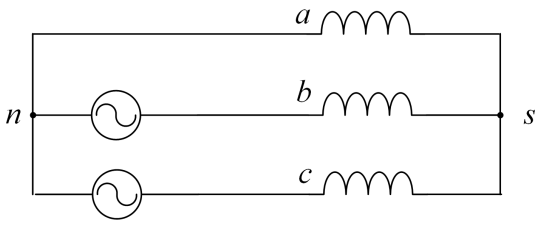

FIGURE 10. Equivalent circuit of the three-phase inverter with $V_{dc_a} = 0$V, $V_{dc_b} = 200$V, and $V_{dc_c} = 200$V.

proposed in [32] and the traditional SVPWM compared to the proposed method.

C. PROPOSED LIMP-HOME MODE OPERATION

The NVM with the proposed method can be applied when there are no remaining modules in one phase. In this case, a weight factor in (15) has an infinite value. Thus, the neutral voltage reference has infinite magnitude in the traditional method [32], and no pole voltage reference is commanded. On the other hand, the method proposed in this paper produces the neutral voltage reference through (29) even under whole modules in a phase are absent, still the MLCI can operate with a limited voltage vector region. This mode is called limp-home mode. Fig. 9 shows that the phase a pole voltage reference is zero, because the neutral voltage reference is equal to the original phase voltage reference of phase a by (29). This is the same as the two-phase modulation principle, and it can be represented as the equivalent circuit shown in Fig. 10. The figure shows that the equivalent circuit of the MLCI when phase a is bypassed after failure. In the figure, the three-phase voltages are obtained as follows:

$$\begin{bmatrix} 0 \\ v_{bn} \\ v_{cn} \end{bmatrix} = \begin{bmatrix} v_{as} + v_{sn} \\ v_{bs} + v_{sn} \\ v_{cs} + v_{sn} \end{bmatrix} \quad v_{sn} = -v_{as}. \tag{30}$$

Therefore, the three-phase output is balanced when the neutral voltage reference is the same as the phase a voltage reference. The neutral voltage reference obtained from (30) is equal to the neutral voltage reference as modified by (29).

In sum, the proposed NVM method can compensate the overmodulation regions of the traditional NVM suggested in [32]. In addition, the proposed NVM algorithm can be applied as the limp-home mode modulation when all modules of one phase are not available.

TABLE 1. Experimental parameters.

Parameters	Values
Load inductor	2mH
Load resistor	20Ω
Switching frequency	15kHz
Phase delay angle of carriers for each cascaded modules	90°
Fundamental frequency of output voltage	60Hz

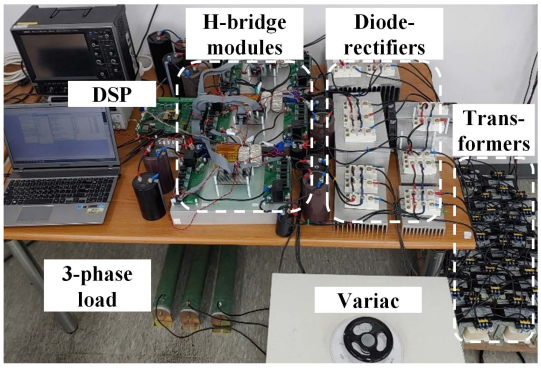

FIGURE 11. Experimental set up: two-by-three MLCI.

D. DUTY REFERENCE CALCULATION

The duty references are calculated as follows:

$$d^*_{p1} = d^*_{p2} = \cdots = d^*_{pN} = \frac{v'_{pn}}{V_{dc\_p}}|_{p\in(a,\,b,\,c)}. \tag{31}$$

These duty references are transmitted to each phase module. Then, the duty references of different polarity are transferred to each leg of the H-bridge to operate with unipolar modulation. Moreover, the carriers of each module are shifted by $180°/N$ to increase the output voltage level.

IV. EXPERIMENTS

Fig. 11 and Table 1 represent the experimental set up and specifications of two-by-three MLCI. To supply the input power to the individual H-bridge inverters, six independent dc-links are fed by one variac, six transformers and diode rectifiers. The MLCI supplies the three-phase RL load consists of 2mH inductor and 20Ω resistor per phase. To implement the control of the MLCI, Texas Instruments' TMS320F28377S digital controller is employed. The internal states of the digital controller are monitered via a 4-channel digital-to-analog converter (DAC) in real-time. The switching frequency is selected to be 15kHz. Since the unipolar modulation is implemented, the effective switching frequency becomes 30kHz for each H-bridge inverter. The carriers of the cascaded modules in the same phase have 90° of phase difference for phase-shifted PWM. All experiments are conducted by applying the maximum phase voltage reference magnitude V_{ph_max} according to the number of modules in each phase, and the fundamental frequency is 60Hz.

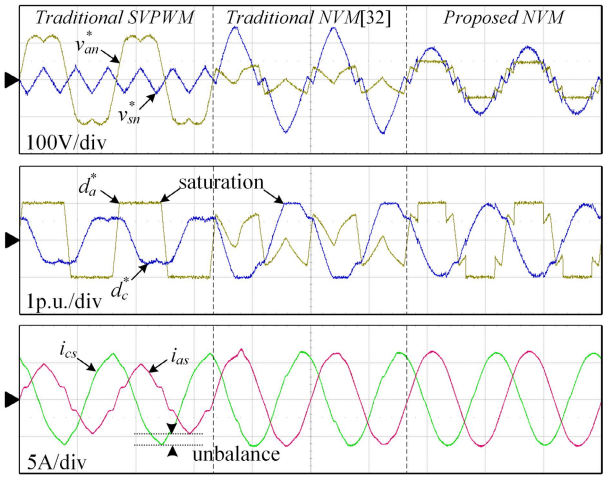

FIGURE 12. Experimental result comparison for the three-phase MLCI with V_{dc_a} = 50V, V_{dc_b} = 200V, and V_{dc_c} = 200V(10ms/div).

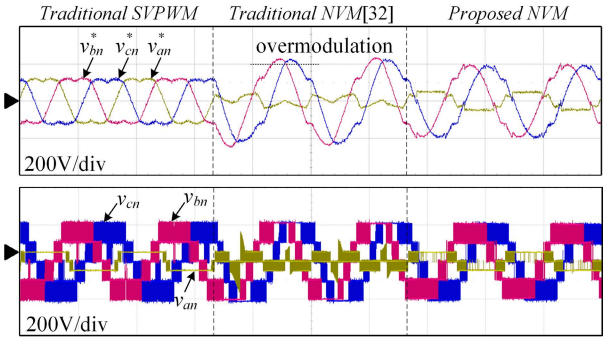

FIGURE 13. Pole voltage comparison for the three-phase MLCI with V_{dc_a} = 50V, V_{dc_b} = 200V, and V_{dc_c} = 200V (10ms/div).

TABLE 2. Comparison of modulation indices.

	Traditional SVPWM	Traditional NVM[32]	Proposed NVM
m_a	2.5	0.72	1
m_b	0.63	1.23	1
m_c	0.63	1.23	1

In asymmetrical condition, each dc-link voltages of two-by-three MLCI are the same as V_{dc_a} = 50V, V_{dc_b} = 200V, V_{dc_c} = 200V when N_a = 1, N_b = 2, and N_c = 2. Fig. 12 compares the waveforms in each modulation method. Compared to traditional SVPWM, the output currents are balanced when the traditional or proposed NVM is applied. In addition, compare to the traditional NVM suggested in [32], the THD of i_{cs} is reduced from 6.25% to 1.75%. Moreover, the THD of i_{as} decreases from 6.97% to 1.79% compared to the traditional NVM. This corresponds that the proposed method improves the THD by 28% compared to traditional NVM.

Fig. 13 shows the comparison of pole voltages v_{an}, v_{bn}, and v_{cn} and their reference voltages for each modulation method. In the traditional SVPWM, v_{an} is almost fully saturated. In the traditional NVM, v_{bn} and v_{cn} are partially saturated, because v^*_{bn} and v^*_{cn} exceed their total dc-link voltage 200V. In the proposed NVM, the saturated regions disappear in v_{bn} and v_{cn} which are normal phases' pole voltages. It means that the healthy phases are not undergoing overmodulation phenomenon. On the other hand, the pole voltage v_{an} is partially constant at 50V and -50V with the proposed NVM, but this is not caused by the overmodulation unlike the traditional SVPWM and traditional NVM.

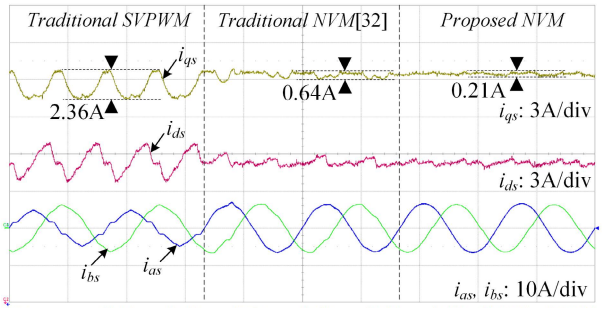

FIGURE 14. *d*- and *q*-axis current responses (10ms/div).

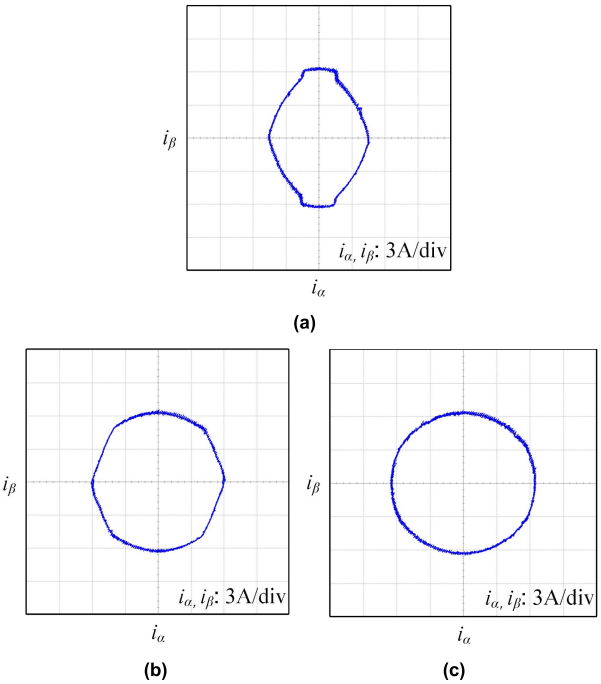

FIGURE 15. Comparison of the current trajectories in the $\alpha\beta$ plane. (a) Traditional SVPWM. (b) Traditional NVM [32]. (c) Proposed NVM.

Table 2 represents the three-phase modulation indices m_a, m_b, and m_c of each modulation method. In the traditional SVPWM, m_a is 2.5. In the traditional NVM, m_b and m_c are 1.23. These mean that the three-phase MLCI operates at the overmodulation region with the traditional SVPWM or the traditional NVM. On the other hand, in the proposed NVM, m_a, m_b, and m_c are 1, so the three-phase MLCI operates at the linear modulation region.

Fig. 14 presents the dq plane currents i_{ds} and i_{qs}. When the proposed NVM is applied, the ripple component of i_{qs} is reduced by 32.8% compared to traditional NVM method.

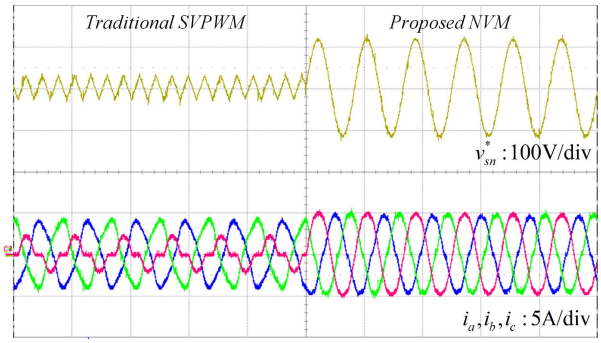

FIGURE 16. Experimental result comparison for the three-phase MLCI with $V_{dc_a} = 0$V, $V_{dc_b} = 200$V, and $V_{dc_c} = 200$V (20ms/div).

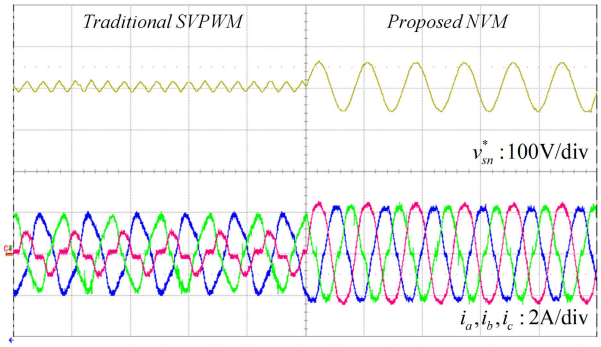

FIGURE 17. Experimental result comparison for the three-phase MLCI with $V_{dc_a} = 0$V, $V_{dc_b} = 100$V, and $V_{dc_c} = 200$V (20ms/div).

Fig. 15 compares the current trajectories of i_α and i_β in the $\alpha\beta$ plane. As can be seen in Figs. 15(a) and 15(b), the trajectory of phase current is distorted when both the traditional SVPWM and NVM proposed in [32] are applied. On the other hand, the shape of the current trajectory in the $\alpha\beta$ plane is much improved with the proposed NVM as shown in Fig. 15(c).

In sum, with the proposed NVM method, the overmodulation region occurred in the traditional NVM suggested in [32] disappears. As a results, the balanced three-phase outputs in the maximum linear modulation region can be obtained by applying the proposed NVM for asymmetrical three-phase MLCI. In addition, the distortion of the output current is mitigated.

The effectiveness of the proposed NVM is also verified when all modules in one phase are bypassed as shown in Figs. 16 and 17. In Fig. 16, the three-phase output currents become well-balanced after the proposed NVM is applied when $V_{dc_a} = 0$V, $V_{dc_b} = 200$V, and $V_{dc_c} = 200$V. Moreover, in Fig. 17, the balanced three-phase output currents are achieved by applying the proposed NVM when $V_{dc_a} = 0$V, $V_{dc_b} = 100$V, and $V_{dc_c} = 200$V. The MLCI operations in both cases are not possible in traditional modulation strategies.

V. CONCLUSION

This paper proposed the improved NVM technique for the post-fault operation of three-phase MLCIs. Compared to the traditional SVPWM and NVM methods, the proposed method maximizes the linear modulation region under severe dc-link voltage imbalance conditions as well as avoiding overmodulations. Moreover, the proposed method can generate balanced three-phase voltage even one phase leg is totally unavailable. With this limp-home mode, the fault tolerant ability of the MLCI is significantly enhanced. The proposed method was tested in two-by-three MLCI prototypes under various dc-link conditions including the limp-home mode. The effectiveness of the proposed method was fully verified through the experimental results.

REFERENCES

[1] M. Vijeh, M. Rezanejad, E. Samadaei, and K. Bertilsson, "A general review of multilevel inverters based on main submodules: Structural point of view," *IEEE Trans. Power Electron.*, vol. 34, no. 10, pp. 9479–9502, Oct. 2019.

[2] J. Rodriguez, L. G. Franquelo, S. Kouro, J. I. Leon, R. C. Portillo, M. Á. M. Prats, and M. A. Perez, "Multilevel converters: An enabling technology for high-power applications," *Proc. IEEE*, vol. 97, no. 11, pp. 1786–1817, Nov. 2009.

[3] E.-J. Lee and K.-B. Lee, "Performance improvement of cascaded H-bridge multilevel inverters with modified modulation scheme," *J. Power Electron.*, vol. 21, no. 3, pp. 541–552, Mar. 2021.

[4] A. R. Kumar and T. Deepa, "Multilevel inverters: A review of recent topologies and new modulation techniques," in *Proc. Int. Conf. Recent Trends Electr., Control Commun. (RTECC)*, Mar. 2018, pp. 196–203.

[5] H. Abu-Rub, J. Holtz, J. Rodriguez, and G. Baoming, "Medium-voltage multilevel converters-state of the art, challenges, and requirements in industrial applications," *IEEE Trans. Ind. Electron.*, vol. 57, no. 8, pp. 2581–2596, Aug. 2010.

[6] M. Marimuthu, S. Vijayalakshmi, and R. Shenbagalakshmi, "A novel non-isolated single switch multilevel cascaded DC–DC boost converter for multilevel inverter application," *J. Elect. Eng. Technol.*, vol. 15, pp. 2157–2166, Aug. 2020.

[7] X. Zhang, T. Zhao, W. Mao, D. Tan, and L. Chang, "Multilevel inverters for grid-connected photovoltaic applications: Examining emerging trends," *IEEE Power Electron. Mag.*, vol. 5, no. 4, pp. 32–41, Dec. 2018.

[8] K. Shen, G. Zhao, and D. Zhao, "Improved fundamental frequency switching control method for MMC based STATCOM considering capacitor voltage ripple," in *Proc. 45th Annu. Conf. IEEE Ind. Electron. Soc. (IECON)*, Oct. 2019, pp. 3349–3354.

[9] A. A. Hafez, A. A. Mahmoud, and A. M. Yousef, "Robust and intelligent control for single-stage grid-connected modular multilevel converter in PV applications," *J. Electr. Eng. Technol.*, vol. 16, no. 2, pp. 917–931, Mar. 2021.

[10] Q. Huo, P. Wang, G. Cao, J. Zhu, J. Yin, X. Guo, and T. Wei, "Novel flexible HVDC transmission converter station topology with DC fault blocking capability," *J. Power Electron.*, vol. 20, no. 4, pp. 884–893, Jul. 2020.

[11] A. Nabae, I. Takahashi, and H. Akagi, "A new neutral-point-clamped PWM inverter," *IEEE Trans. Ind. Appl.*, vol. IA-17, no. 5, pp. 518–523, Sep. 1981.

[12] J.-S. Lai and F. Z. Peng, "Multilevel converters-a new breed of power converters," *IEEE Trans. Ind. Appl.*, vol. 32, no. 3, pp. 509–517, May/Jun. 1996.

[13] M. Chai, N. B. Y. Gorla, and S. K. Panda, "Fault detection and localization for cascaded H-bridge multilevel converter with model predictive control," *IEEE Trans. Power Electron.*, vol. 35, no. 10, pp. 10109–10120, Oct. 2020.

[14] D. Ronanki and S. S. Williamson, "Modular multilevel converters for transportation electrification: Challenges and opportunities," *IEEE Trans. Transport. Electrific.*, vol. 4, no. 2, pp. 399–407, Jun. 2018.

[15] Y. Liu, Y. Liu, Y. Jin, and J. Chen, "Novel submodule voltage balancing topology for hybrid modular multilevel converters," *J. Power Electron.*, vol. 21, no. 10, pp. 1416–1426, Oct. 2021.

[16] H. Mhiesan, Y. Wei, Y. P. Siwakoti, and H. A. Mantooth, "A fault-tolerant hybrid cascaded H-bridge multilevel inverter," *IEEE Trans. Power Electron.*, vol. 35, no. 12, pp. 12702–12715, Dec. 2020.

[17] P. W. Hammond, "Enhancing the reliability of modular medium-voltage drives," *IEEE Trans. Ind. Electron.*, vol. 49, no. 5, pp. 948–954, Oct. 2002.

[18] J. Rodriguez, P. W. Hammond, J. Pontt, R. Musalem, P. Lezana, and M. J. Escobar, "Operation of a medium-voltage drive under faulty conditions," *IEEE Trans. Ind. Electron.*, vol. 52, no. 4, pp. 1080–1085, Aug. 2005.
[19] P. M. Lingom, J. Song-Manguelle, J. M. Nyobe-Yome, D. L. Mon-Nzongo, T. Jin, and M. L. Doumbia, "Control of a cascaded H-bridge multilevel inverter with failed cells for grid-connected application," in *Proc. IEEE 10th Int. Symp. Power Electron. Distrib. Gener. Syst. (PEDG)*, Jun. 2019, pp. 806–811.
[20] P. Lezana and G. Ortiz, "Extended operation of cascade multicell converters under fault condition," *IEEE Trans. Ind. Electron.*, vol. 56, no. 7, pp. 2697–2703, Jul. 2009.
[21] P. M. Lingom, J. Song-Manguelle, D. L. Mon-Nzongo, R. C. C. Flesch, and T. Jin, "Analysis and control of PV cascaded H-bridge multilevel inverter with failed cells and changing meteorological conditions," *IEEE Trans. Power Electron.*, vol. 36, no. 2, pp. 1777–1789, Feb. 2021.
[22] S. Farzamkia, H. Iman-Eini, M. Noushak, and A. Hadizadeh, "Improved fault-tolerant method for modular multilevel converters by combined DC and neutral-shift strategy," *IEEE Trans. Ind. Electron.*, vol. 66, no. 3, pp. 2454–2462, Mar. 2019.
[23] Z. Ni, A. H. Abuelnaga, and M. Narimani, "A new fault-tolerant technique based on nonsymmetrical selective harmonic elimination for cascaded H-bridge motor drives," *IEEE Trans. Ind. Electron.*, vol. 68, no. 6, pp. 4610–4622, Jun. 2021.
[24] L. Maharjan, T. Yamagishi, H. Akagi, and J. Asakura, "Fault-tolerant operation of a battery-energy-storage system based on a multilevel cascade PWM converter with star configuration," *IEEE Trans. Power Electron.*, vol. 25, no. 9, pp. 2386–2396, Sep. 2010.
[25] S.-M. Kim, J.-S. Lee, and K.-B. Lee, "A modified level-shifted PWM strategy for fault-tolerant cascaded multilevel inverters with improved power distribution," *IEEE Trans. Ind. Electron.*, vol. 63, no. 11, pp. 7264–7274, Nov. 2016.
[26] Q. Zeng, F. Xiao, Q. Ren, and S. Ai, "Modulation signal analysis and parameter selection for modular multi-level converters with harmonic injection method," *J. Power Electron.*, vol. 20, no. 2, pp. 455–465, Mar. 2020.
[27] J. Kim and Y. Cho, "Improved neutral shift method for fault tolerant operation of three phase MLCI," *J. Power Electron.*, vol. 21, no. 1, pp. 49–58, Jan. 2021.
[28] R. Sharma and A. Das, "Extended reactive power exchange with faulty cells in grid-tied cascaded H-bridge converter for solar photovoltaic application," *IEEE Trans. Power Electron.*, vol. 35, no. 6, pp. 5683–5691, Jun. 2020.
[29] R. Sharma and A. Das, "Postfault operation of cascaded H-bridge converter for equal power handling by the healthy cells," *IEEE Trans. Ind. Electron.*, vol. 67, no. 11, pp. 9174–9183, Nov. 2020.
[30] F. Carnielutti, H. Pinheiro, and C. Rech, "Generalized carrier-based modulation strategy for cascaded multilevel converters operating under fault conditions," *IEEE Trans. Ind. Electron.*, vol. 59, no. 2, pp. 679–689, Feb. 2012.
[31] S. Ouni, M. R. Zolghadri, M. Khodabandeh, M. Shahbazi, J. Rodríguez, and H. Oraee, "Improvement of post-fault performance of a cascaded H-bridge multilevel inverter," *IEEE Trans. Ind. Electron.*, vol. 64, no. 4, pp. 2779–2788, Apr. 2017.
[32] Y. Cho, T. LaBella, J.-S. Lai, and M. K. Senesky, "A carrier-based neutral voltage modulation strategy for multilevel cascaded inverters under unbalanced DC sources," *IEEE Trans. Ind. Electron.*, vol. 61, no. 2, pp. 625–636, Feb. 2014.

JEONGWOO KIM (Member, IEEE) was born in Seoul, South Korea, in 1989. He received the B.S. and Ph.D. degrees in electrical engineering from Konkuk University, Seoul, in 2014 and 2021, respectively. Since 2021, he has been with the Department of Electrical and Electronics Engineering, Konkuk University, where he is currently working as an Assistant Professor. His current research interests include fault tolerant operation techniques for power electronic converters and multi-level converters.

YOUNGHOON CHO (Member, IEEE) was born in Seoul, South Korea, in 1980. He received the B.S. degree in electrical engineering from Konkuk University, Seoul, in 2002, the M.S. degree in electrical engineering from Seoul National University, Seoul, in 2004, and the Ph.D. degree from the Virginia Polytechnic Institute and State University, Blacksburg, VA, USA, in 2012. From 2004 to 2009, he was an Assistant Research Engineer at the Hyundai MOBIS Research and Development Center, Yongin, South Korea. Since 2013, he has been with the Department of Electrical and Electronics Engineering, Konkuk University, where he is currently working as an Associate Professor. His current research interests include digital control techniques for the power electronic converters in vehicle and grid applications, multi-level converters, and high-performance motor drives.